Optimize ISAR Imaging Techniques for Diverse Moving Targets

Yahya Abdulgader Elgadi
Electrical and Electronic Engineering Departement
Univerversity of Tripoli
Tripoli; Libya
y.elgadi@uot.edu.ly

Adel Saad Emhemmed
Electrical and Electronic Engineering Departement
Univerversity of Tripoli
Tripoli; Libya
dr.adel.elec@gmail.com

Ibrahim Asaad Aref
School of Computing and Communications
Lancaster University
Lancaster, UK
i.aref@lancaster.ac.uk

***Abstract*—ISAR has emerged as a powerful tool within radar technology, specifically designed for imaging and analyzing moving targets. Unlike conventional radar systems, ISAR leverages the motion of the target itself to create high-resolution images. This work explores the methodology and implementation of ISAR imaging, with a specific emphasis on both simple and complex objects, including cubes, spheres, and aircraft. The study investigates three distinct cases, examining the impact of optimum design procedures, variations in center frequency, and alterations in resolution. The main objective of this paper is to optimize ISAR imaging techniques for diverse moving targets, highlighting the importance of adhering to best practices in radar system design. The study demonstrates the effectiveness of optimum design procedures in achieving high-fidelity ISAR images. The results underscore the critical role of resolution in capturing precise and informative ISAR images, providing valuable insights for future advancements in radar technology and imaging systems for moving targets.**

Keywords—ISAR, Optimize, Simulation, Radar

I. INTRODUCTION

Within the broader context of synthetic aperture radar (SAR), Inverse Synthetic Aperture Radar (ISAR) imaging stands out as a specialized approach. While traditional SAR primarily serves Earth remote sensing purposes, ISAR focuses on imaging and characterizing dynamic targets such as aircraft, ships, or ground vehicles. The technique cleverly utilizes the intrinsic motion of the target to virtually create an extended antenna aperture, enabling the generation of high-resolution two-dimensional images even in the presence of target motion [1]. By collecting and processing radar reflections from a moving target over multiple observations, ISAR systems produce detailed images that provide valuable insights into the target's shape, orientation, and structural features. This capability is particularly invaluable in applications such as military surveillance, maritime vessel identification, and aerospace object recognition, where precise analysis and identification of moving targets are crucial [2].

In recent decades, ISAR imaging has emerged as a focal point in radar imaging, garnering significant attention due to its unique capabilities and versatile applications [3]. This technique delivers high-resolution images that enable comprehensive analysis and recognition of intricate target features. Notably, ISAR excels in imaging non-cooperative targets, facilitating the detection and tracking of objects attempting to evade radar systems [4]. The integration of target motion compensation algorithms in ISAR techniques further enhances its utility, allowing the generation of focused images even when both the target and the radar platform are in motion. This adaptability makes ISAR imaging particularly suitable for scenarios involving moving targets, such as airborne or maritime surveillance [5].

Moreover, ISAR imaging significantly contributes to signature analysis by providing valuable insights into a target's radar cross-section (RCS) at various aspect angles. This information is critical for assessing detectability and vulnerability. The ongoing advancements in signal processing techniques and radar technology have substantially improved the efficiency and practicality of ISAR imaging [4]. As a result, its relevance has grown across diverse domains, including military operations, aerospace exploration, maritime activities, and environmental monitoring [7]. The main aim of this work is to investigate and analyze the methodology involved in ISAR processing, including data collection, signal processing, and image generation, and then conduct simulations of ISAR imaging and carefully analyze the results to evaluate the effectiveness and performance of the technique.

II. DESIGN PROCEDURE FOR ISAR IMAGING

The key point for a successful ISAR image is to start the procedure by selecting the ISAR image size, that is, range and cross-range window extends. If the range window extend is x_max and the cross-range window extend is y_max, then the size of the ISAR image, x_max by y_max, should be selected to cover the actual size of the target to be imaged. It is important to note that the size of the target changes in the ISAR image according to the look angle of the radar. The other key selection is the range and cross-range resolutions, Δx and Δy, respectively. These numbers are so critical that they define how many pixels will lie on the target. Therefore, these resolutions are linked to the quality of the ISAR image. After the resolutions in the ISAR image are decided, the sampling points in range, N_X , and the sampling points in cross-range, N_Y can be calculated using the formulas below:

$$N_X = \frac{\Delta x}{x_{max}}. \qquad N_y = \frac{\Delta y}{y_{max}}. \tag{1}$$

After that, once the ISAR size is determined, the resolutions in frequency, Δf , and aspect, $\Delta \phi$, can be determined by utilizing the Fourier relationships between frequency and range and between angle-and-cross-range as demonstrated below:

$$\Delta f = \frac{B}{N_x} = \frac{c/_2}{x_{max}}. \quad , \quad \Delta \phi = \frac{\Omega}{N_y} = \frac{\lambda_c/_2}{y_{max}}. \tag{2}$$

$$B = N_x.\Delta f = \frac{N_x.c}{2.x_{max}}. \quad \Omega = N_y.\Delta \phi = \frac{N_y.\lambda_c}{2.y_{max}}. \tag{3}$$

If the frequencies will be centered around f_c and the radar look angles will be centered around, the ϕ_C then the backscattered electric field should be collected for the following multiple frequencies and angles.

$$\boldsymbol{f} = \left[\left(f_c - \frac{N_x \Delta f}{2}\right)\left(f_c - \left(\frac{N_x}{2} - 1\right).\Delta f\right) \ldots (f_c) \ldots \left(f_c + \left(\frac{N_x}{2} - 1\right).\Delta f\right)\right]_{1\times N_x}. \quad (4)$$

$$\phi = \left[\left(\phi_c - \frac{N_y \Delta \phi}{2}\right)\left(\phi_c - \left(\frac{N_y}{2} - 1\right).\Delta \phi\right) \ldots (\phi_c) \ldots \left(\phi_c + \left(\frac{N_y}{2} - 1\right).\Delta \phi\right)\right]_{1\times N_y}. \quad (5)$$

At this last step, we can take the 2D IFT to get the final ISAR image. If the backscattered field data are collected within a small frequency bandwidth and the angles, then IDFT can be readily applied. The basic flowchart for designing an ISAR image is given in Figure 1. The steps of the algorithm are given briefly in order:

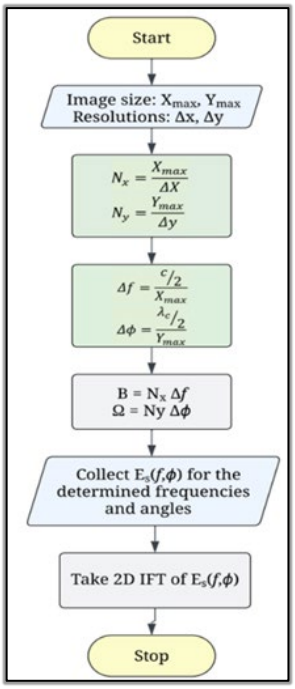

Fig. 1 Flowchart for the basic ISAR imaging algorithm.

III. ISAR Simulation Results and Discussion

This section focuses on simulating ISAR images with ANSYS Electronics HFSS 2022. The main objective is to examine the complex process of ISAR imaging through the simulation of radar returns generated by a range of geometric shapes, encompassing basic forms such as boxes, cylinders, and spheres. By exploiting HFSS's simulation capabilities [6], in this section, we tried examining the impact of diverse factors, including geometric configurations, resolution, bandwidth, and frequencies, on the ending ISAR images. The objective of these simulations is to offer insights into the procedure of acquiring high-resolution ISAR images for basic shapes, explaining the influence of different factors on radar returns and the subsequent imaging process.

In this section, the focus is on the ISAR Imaging Simulation for simple objects, namely a cube and a sphere, and a complex object, which is Air Craft. The main aim is to explore the intricacies of ISAR imaging through a comprehensive analysis of three distinct cases for each object. The primary case involves an optimized design procedure to showcase the highest quality ISAR images for each object. In contrast, the other two cases delve into the imaging process without implementing the optimum design procedure, allowing for a comparative study of the impact of design choices on the resulting ISAR images. Through this exploration, the section seeks to provide valuable insights into the importance of optimal design considerations in achieving high-fidelity ISAR images for simple geometric shapes.

A. Cube Imaging

The 3d model view of a cube whose ISAR image is going to be constructed is shown in Figure 2 The dimensions of the cube are 10, 8, and 8m in x, y, and z directions, respectively.

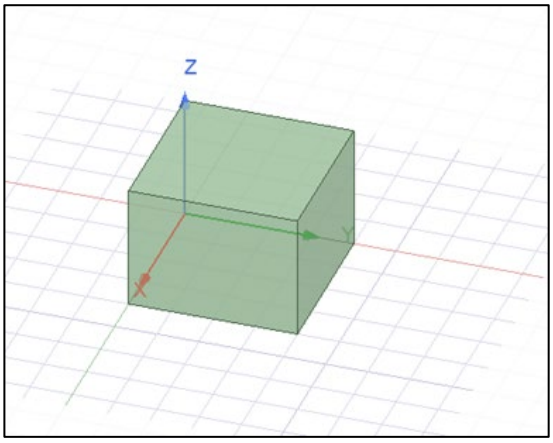

Fig. 2 Cube model in HFSS environment

Case 1: Optimized Design Procedure: Since the cube size is 10, 8m, the image window should be chosen so that it would cover the whole cube on the 2D x–y plane. Therefore, the size of the image is set at 10, and 10m in the *x* and *y* directions, respectively. The center frequency is chosen to be 35GHz so that the cube is considered a large structure compared to the Radar's wavelength. Then, the range and cross-range resolutions are set as follows $\Delta x = 10\ cm$ and $\Delta y = 10\ cm$, respectively. Therefore, the sampling points in the range (N_x) and the sampling points in cross-range (N_y) will be equal to:

$$N_X = \frac{x_{max}}{\Delta x} = \frac{10}{0.1} = 100 \quad (6)$$

$$N_y = \frac{y_{max}}{\Delta y} = \frac{10}{0.1} = 100 \quad (7)$$

Now, we can determine the frequency resolution, Δf, aspect resolution, $\Delta \phi$, bandwidth B and aspect range Ω from the following equations:

$$\Delta f = \frac{B}{N_x} = \frac{c/2}{x_{max}} = \frac{c}{20} = 15MHz \quad (8)$$

$$\Delta\phi = \frac{\Omega}{N_y} = \frac{\lambda_c/2}{y_{max}} = \frac{0.008}{20} = 0.0245° \quad (9)$$

$$B = N_x.\Delta f = \frac{N_x.c}{2.x_{max}} = 100 \times 15M = 1.5GHz \quad (10)$$

$$\Omega = N_y.\Delta\phi = \frac{N_y.\lambda_c}{2.y_{max}} = 100 \times 0.0245° = 2.45° \quad (11)$$

Once the above quantities are defined, the backscattered electric field should be collected for frequencies from 34.25 to 35.75 GHz for a total of 100 discrete frequencies and from −1.22° to 1.23° for 100 distinct azimuth angles. Therefore, the simulation of the cube is obtained by calculating the backscattered electric field $E_s(f, \varphi)$ for these frequencies and

angles. At the end of the simulation, 2D multifrequency multi-aspect backscattered field data of size 100 by 100 are obtained. Lastly, by taking the 2-D IFT for the data collected the ISAR image demonstrated in Figure 3 is obtained.

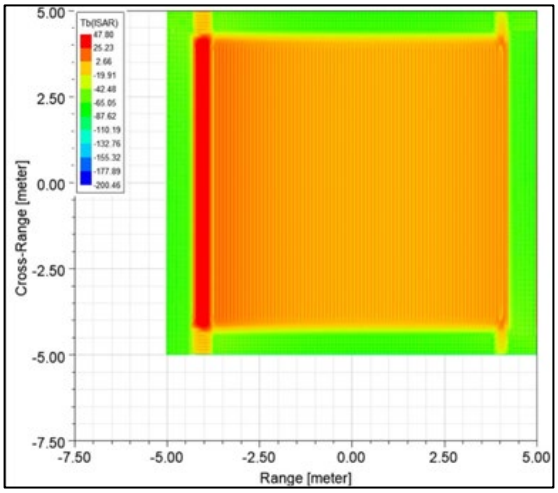

Fig. 3: 2-D ISAR image for a cube with a 35GHz center frequency.

The ISAR image of the cube successfully represents both cross-range (y-axis) and range (x-axis) dimensions accurately. The geometric features of the cube appear well-defined, and the electric field distribution aligns with the expected behavior for a cube of dimensions 10, and 8m.

Case 2: Frequency Effects on ISAR Imaging: it examines the impact of changing the center frequency, leading to a situation where the structure size is no longer considered large compared to the radar's wavelength. This occurs when the condition stating that the length of the structure is smaller than 1000 times the wavelength ($1000\lambda_c$) is not satisfied. The size of the cube is held constant as a center frequency of 10GHz is chosen, resulting in changes to both the aspect resolution, $\Delta\phi$, and the aspect range, Ω. These changes are determined by the following equations:

$$\Delta\phi = \frac{\Omega}{N_y} = \frac{\lambda_c/_2}{y_{max}} = \frac{0.03}{20} = 0.0859° \quad (12)$$

$$\Omega = N_y.\Delta\phi = \frac{N_y.\lambda_c}{2.y_{max}} = 100 \times 0.0859° = 8.59° \quad (13)$$

The aforementioned parameters being established, the backscattered electric field is gathered across a frequency range of 9.25 to 10.75 GHz, encompassing 100 discrete frequencies, and across azimuth angles ranging from -4.3° to 4.29°, with 100 distinct angles. Consequently, the simulation of the cube involves computing the backscattered electric field, denoted as $E_s(f, \varphi)$ for these specified frequencies and angles. Upon completing the simulation, a 2D multifrequency multi-aspect backscattered field dataset, sized at 100 by 100, is obtained. Figure 4 illustrates the two-dimensional Inverse Fourier Transform applied to the collected data, presenting the resulting ISAR image.

The ISAR image obtained by decreasing the center frequency to 10 GHz, thereby increasing the wavelength and shifting the cube from a large to a smaller structure relative to the wavelength, manifests as a uniformly red image. This uniform red coloration across the entire image signifies an intense electric field with minimal variation, suggesting a prevalence of backscattering effects. The altered size-to-wavelength ratio influences the scattering characteristics, leading to a dominant representation of overall intensity rather than distinct details on the cube's surface. The lack of detailed features in the ISAR image underscores the challenges posed by imaging smaller structures at lower frequencies, where limited resolution capabilities impede the system's ability to capture finer details.

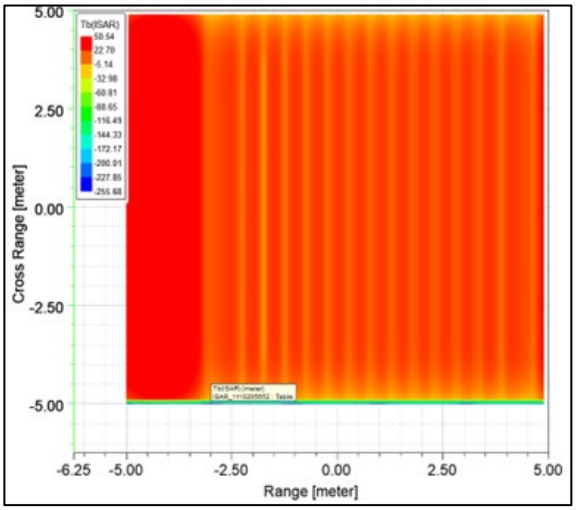

Fig. 4: 2-D ISAR image for a cube with a 10GHz center frequency.

Case 3: Resolution Effects on ISAR Imaging: it examines the impact of modifying range and cross-range resolutions. In the initial step, resolutions are established at $\Delta x = 50cm$ and $\Delta y = 50cm$, resulting the sampling points in range (N_X) and the sampling points in cross-range (N_y) to be equal to:

$$N_X = \frac{x_{max}}{\Delta x} = \frac{10}{0.5} = 20 \quad (14)$$

$$N_y = \frac{y_{max}}{\Delta y} = \frac{10}{0.5} = 20 \quad (15)$$

In the second step, considering a cube size of 10, 8m, an image window measuring 10 by 10m is selected to encompass the entire cube on the 2D x–y plane. To maintain the cube as a large structure relative to the radar's wavelength, the center frequency is set at 37GHz. In the following step, various parameters, including frequency resolution (Δf), aspect resolution ($\Delta\phi$), bandwidth (B), and aspect range (Ω), are determined using specific equations as follows:

$$\Delta f = \frac{B}{N_x} = \frac{c/_2}{x_{max}} = \frac{c}{20} = 15MHz \quad (16)$$

$$\Delta\phi = \frac{\Omega}{N_y} = \frac{\lambda_c/_2}{y_{max}} = \frac{0.008}{20} = 0.0245° \quad (17)$$

$$B = N_x.\Delta f = \frac{N_x.c}{2.x_{max}} = 20 \times 15M = 0.3GHz \quad (18)$$

$$\Omega = N_y.\Delta\phi = \frac{N_y.\lambda_c}{2.y_{max}} = 20 \times 0.0245° = 0.49° \quad (19)$$

Subsequent to these calculations, the backscattered electric field is collected for frequencies ranging from 34.85 to 35.145 GHz and azimuth angles from -0.245° to 1.23°, resulting in 20 discrete frequencies and angles. The simulation yields a 2D multifrequency multi-aspect backscattered field dataset sized at 20 by 20. Finally, applying the 2-D Inverse

Fourier Transform to the collected data produces the ISAR image, as depicted in Figure 5.

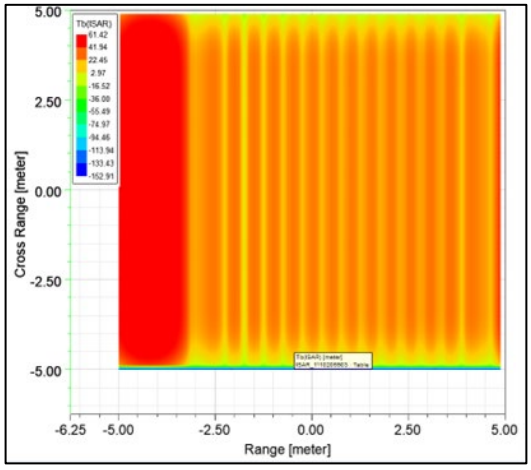

Fig. 5: 2-D ISAR image for a cube with a center frequency of 35GHz and $\Delta x = \Delta y = 50\ cm$.

The ISAR image of the cube, obtained by decreasing the resolution to 0.5m from 0.1m and reducing the number of samples from 100 to 20, reveals intriguing characteristics. The visual representation showcases a red line amidst separated yellow lines, with the red line denoting an intense electric field, corresponding to a strong scattering. The separated yellow lines suggest regions of less intense electric field, indicative of reduced scattering or reflection. The decrease in spatial resolution introduces spatial smearing and averaging effects, leading to the formation of distinct lines in the ISAR image. This outcome underscores the impact of resolution choices on the clarity and interpretation of the resulting image, highlighting the trade-offs between resolution, computational efficiency, and image fidelity.

B. Sphere Imaging

Figure 6 presents a 3D model featuring a sphere with an 8-meter diameter. Positioned at the center of the coordinate system with coordinates 0, 0, 0 in the x, y, and z directions, this sphere will be the subject for the upcoming creation of its ISAR image.

Case 1: Optimized Design Procedure: in the first step, we need to encompass the entire 8-meter diameter sphere on the 2D x–y plane, select an image window size of 10 by 10 meters in the x and y directions, respectively. The center frequency is designated as 37GHz to ensure the sphere qualifies as a large structure relative to the radar's wavelength. After that, establish range and cross-range resolutions at $\Delta x = 5cm$ and $\Delta y = 5cm$ for the sphere. Consequently, the number of sampling points in both range (N_X)and cross-range (N_y) equals:

$$N_X = \frac{x_{max}}{\Delta x} = \frac{10}{0.05} = 200 \quad (20)$$

$$N_y = \frac{y_{max}}{\Delta y} = \frac{10}{0.05} = 200 \quad (21)$$

Now, we can determine the frequency resolution, Δf, aspect resolution, Δϕ, bandwidth B and aspect range Ω from the following equations:

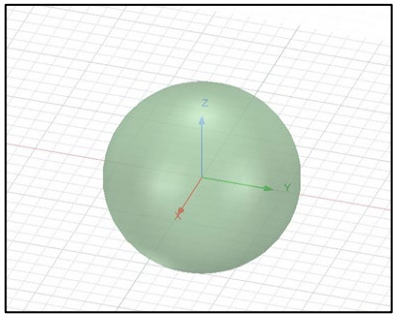

Fig. 6: Sphere model in HFSS environment.

$$\Delta f = \frac{B}{N_x} = \frac{c/2}{x_{max}} = \frac{c}{20} = 15MHz \quad (22)$$

$$\Delta\phi = \frac{\Omega}{N_y} = \frac{\lambda_c/2}{y_{max}} = \frac{0.0081}{20} = 0.0232° \quad (23)$$

$$B = N_x.\Delta f = \frac{N_x.c}{2.x_{max}} = 200 \times 15M = 3GHz \quad (24)$$

$$\Omega = N_y.\Delta\phi = \frac{N_y.\lambda_c}{2.y_{max}} = 200 \times 0.0245° = 4.9° \quad (25)$$

Then, we need to define the mentioned parameters and proceed to collect the backscattered electric field for frequencies spanning from 35.5 to 38.5 GHz, totaling 200 discrete frequencies. Additionally, collect data from azimuth angles ranging from -2.45° to 2.45° with 200 distinct angles. This simulation involves calculating the backscattered electric field, $E_s(f, \phi)$, for the specified frequencies and angles. Following the simulation, a 2D multifrequency multi-aspect backscattered field dataset sized at 200 by 200 is generated. Finally, applying the 2-D Inverse Fourier Transform to the collected data yields the ISAR image showcased in Figure 7.

Figure 7 presents an ISAR image of a sphere obtained through an optimum design procedure. The image reveals a notable characteristic whereby the sphere's shape is accurately depicted as a circle for approximately half of the image area. However, a portion of the image exhibits an overlapping effect, which can be attributed to the inherent challenges associated with imaging spherical objects.

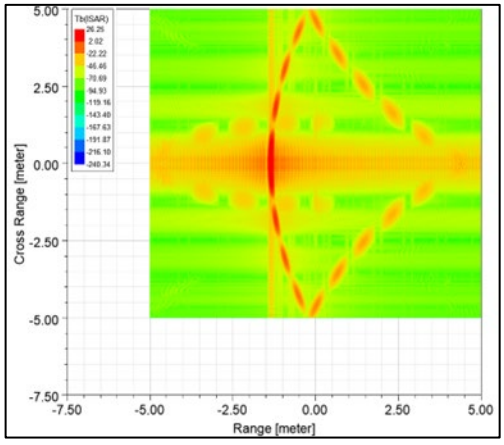

Fig. 7: 2-D ISAR image for a sphere with a 37GHz center frequency.

One primary factor contributing to the observed overlap is the limited availability of a wide range of aspect angles in the simulation of this image. Due to practical limitations, simulating a wide range of aspect angles can be challenging,

as it would require a significant number of samples and a broad bandwidth. The presented ISAR image provides valuable insights into the imaging difficulties encountered when reconstructing the shape of a sphere.

Case 2: Frequency Effects on ISAR Imaging: here the main objective is to investigate the impact of changing the center frequency is examined, resulting in a situation where the structure size is no longer considered large relative to the radar's wavelength. This occurs when the condition stipulating that the length of the structure is smaller than 1000 times the wavelength is not satisfied. Keeping the size of the sphere constant, a center frequency of 10GHz is chosen, leading to changes in both the aspect resolution, $\Delta\phi$, and the aspect range, Ω. These changes are determined by the following equations:

$$\Delta\phi = \frac{\Omega}{N_y} = \frac{\lambda_c/_2}{y_{max}} = \frac{0.03}{20} = 0.0859° \quad (26)$$

$$\Omega = N_y.\Delta\phi = \frac{N_y.\lambda_c}{2.y_{max}} = 100 \times 0.0859° = 8.59° \quad (27)$$

Having established the previously mentioned parameters, the backscattered electric field is collected over a frequency range spanning from 9.25 to 10.75 GHz, encompassing 200 distinct frequencies, and across azimuth angles ranging from -4.295° to 4.295°, with 200 discrete angles. Subsequently, the cube simulation entails the computation of the backscattered electric field, denoted as $E_s(f,\phi)$,for the specified frequencies and angles.

Following the simulation, a 2D multifrequency multi-aspect backscattered field dataset is obtained, measuring 200 by 200. The resulting data undergoes a two-dimensional Inverse Fourier Transform, as illustrated in Figure 8, revealing the corresponding ISAR image. Figure 8 presents an ISAR image of a sphere obtained at a frequency below the optimum frequency, where the wavelength is larger than the maximum length of the imaged object by a factor of 1000. The image exhibits certain challenges and characteristics that differ from the previous image that shown in Figure 7. A noticeable feature is that the shape of the sphere is depicted as a circle for less than half of the image area. This suggests that the imaging system is not effectively capturing the complete shape of the sphere. Additionally, the lines representing the sphere in the image appear to be larger compared to the previous image that illustrated in Figure 7, indicating a decrease in resolution.

Similar to Figure 7, the image in Figure 8 also exhibits overlapping artifacts, which can be attributed to the inherent limitations associated with imaging spherical objects. As mentioned earlier. However, at a frequency below the optimum frequency, the imaging system lacks the ability to resolve fine details due to the larger wavelength and reduced resolution.

Case 3: Resolution Effects on ISAR Imaging: it examines the impact of modifying range and cross-range resolutions. In the initial step, resolutions are established at Δx=50cm and Δy=50cm, resulting the sampling points in the range (N_X) and the sampling points in cross-range (N_y) to be equal to:

$$N_X = \frac{x_{max}}{\Delta x} = \frac{10}{0.5} = 20 \quad (28)$$

$$N_y = \frac{y_{max}}{\Delta y} = \frac{10}{0.5} = 20 \quad (29)$$

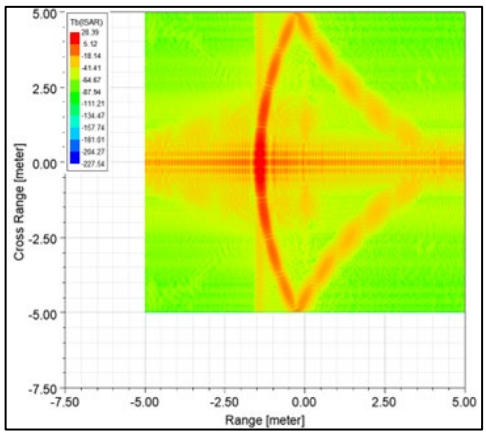

Fig. 8: 2-D ISAR image for a cube with a 10GHz center frequency.

As part of the second stage, and with a sphere with a diameter of 8 meters in mind, a 10 by 10-meter image window is chosen. This selection ensures the complete coverage of the entire sphere on the 2D x–y plane. To uphold the sphere's classification as a substantial structure relative to the radar's wavelength, the center frequency is established at 37GHz. Subsequently, in the ensuing stage, distinct parameters namely, frequency resolution (Δf), aspect resolution ($\Delta\phi$), bandwidth (B), and aspect range (Ω) are computed using specified equations, outlined as follows:

$$\Delta f = \frac{B}{N_x} = \frac{c/_2}{x_{max}} = \frac{c}{20} = 15MHz \quad (30)$$

$$\Delta\phi = \frac{\Omega}{N_y} = \frac{\lambda_c/_2}{y_{max}} = \frac{0.0081}{20} = 0.0232°. \quad (31)$$

$$B = N_x.\Delta f = \frac{N_x.c}{2.x_{max}} = 20 \times 15M = 0.3GHz. \quad (32)$$

$$\Omega = N_y.\Delta\phi = \frac{N_y.\lambda_c}{2.y_{max}} = 20 \times 0.0245° = 0.49° \quad (33)$$

Subsequent to these calculations, the backscattered electric field is collected for frequencies ranging from 36.85 to 37.15 GHz and azimuth angles from -0.245° to 0.245°, resulting in 20 discrete frequencies and angles. The simulation yields a 2D multifrequency multi-aspect backscattered field dataset sized at 20 by 20. Finally, applying the 2-D Inverse Fourier Transform to the collected data produces the ISAR image, as depicted in Figure 9 which presents an ISAR image of a sphere with a significantly reduced resolution, where the image resolution is decreased from 5 cm to 50 cm. The image exhibits distortion and fails to depict any expected shape resembling a sphere or any discernible object. The reduced resolution significantly limits the system's ability to capture the necessary spatial information, resulting in a distorted and unrecognizable image.

The information obtained from previous cases highlights the challenges associated with obtaining an ISAR image for spheres, ball-like shapes, or cylinders which can present certain challenges compared to other object shapes. These challenges arise due to factors such as the lack of distinct scattering centers on their smooth surfaces, resulting in limited spatial information for reconstruction. The symmetrical nature of these objects can introduce ambiguity and overlapping reflections, further complicating the image reconstruction process. Additionally, obtaining a wide range of aspect angles

can be challenging, limiting the available data for comprehensive imaging.

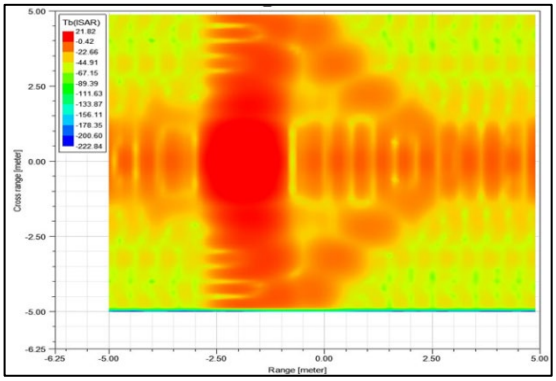

Fig. 9: 2-D ISAR image for a sphere with a center frequency of 37GHz and $\Delta x = \Delta y = 50$ cm.

C. *ISAR Imaging Simulation for Complex Objects*

In this section, the emphasis is on ISAR Imaging Simulation applied to complex objects, such as aircrafts fighter jets. The aim is to thoroughly investigate the nuances of ISAR imaging by conducting a detailed analysis of three distinct scenarios for each object. The primary scenario involves a refined design approach that aims to showcase the highest quality ISAR images for each object. This optimized strategy is intended to demonstrate the production of top-quality ISAR images for each complex object. Conversely, the other two scenarios explore the imaging process without employing the optimal design procedure, enabling a comparative examination of the influence of design choices on the resulting ISAR images. Through this exploration, the section aims to offer valuable insights into the significance of optimal design considerations in achieving high-fidelity ISAR images for intricate objects. This section aims to explore the ISAR imaging of complex objects through the following three distinct study cases:

Case 1: In this case, the focus will be on employing an optimum design procedure to obtain high-fidelity ISAR images, ensuring the application of best practices for capturing intricate details of the object.

Case 2: This case involves deliberately reducing the center frequency below the optimal frequency, resulting in a larger wavelength. By doing so, the impact of a larger wavelength on the resulting ISAR image will be examined, shedding light on the trade-offs and limitations associated with such frequency selections for complex objects.

Case 3: The third case will revolve around decreasing the resolution of the ISAR image. By intentionally reducing the resolution, the effects on the level of detail and accuracy in capturing the features of complex objects will be assessed. This case aims to highlight the significance of resolution in obtaining precise and informative ISAR images of various complex objects.

Throughout these study cases, valuable insights will be gained regarding the ISAR imaging techniques and considerations applicable to a wide range of complex objects, facilitating a deeper understanding of their characteristics and the factors influencing the quality of their ISAR images.

Aircraft and fighter jets present unique challenges in terms of their intricate geometries and complex radar cross-sections. ISAR imaging provides a means to overcome these challenges by capturing radar reflections from multiple perspectives and reconstructing high-resolution images of the objects of interest. By analyzing ISAR images of aircrafts and fighter jets, valuable insights can be gained into their structural features, surface characteristics, and potential areas of interest for further analysis. This section focuses on the application of ISAR imaging techniques to capture detailed information about three specific models: The Bell Boeing, MQ-1 Predator, and a Boeing AH-64 Apache Helicopter.

1) *Bell Boeing V-22 Imaging*

The Bell Boeing V-22 Osprey, a highly versatile tiltrotor military aircraft, serves as the focal point for the construction of its Inverse Synthetic Aperture Radar (ISAR) image. Figure 10 presents an intricate 3D model representation of the V-22 Osprey, offering a comprehensive visualization of its design and structural features. With dimensions of X_max=9m for length and Y_max=12.5m for width, this model provides a valuable reference for generating a precise ISAR image of the aircraft.

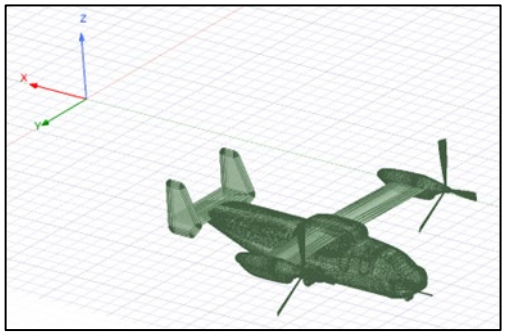

Fig. 10: Bell Boeing V-22 aircraft model in HFSS environment.

This section will explore the ISAR imaging of the Bell Boeing V-22 aircraft through three distinct study cases. Table I reveals the parameters of the three study cases.

Table I: Design parameters of Bell Boeing V-22 aircraft for each of the study cases.

	Case (1)	Case (2)	Case (3)
Center Frequency f_c	25 GHz	7 GHz	25 GHz
Image Size Range X	20m	20m	20m
Image Size Range Y	20m	20m	20m
Range Resolution Δx	0.2m	0.2m	1m
Cross Range Resolution Δy	0.2m	0.2m	1m
Bandwidth B	749.5MHz	749.5MHz	149.9MHz
Aspect Range Ω	1.717°	6.134°	0.3435°
Range sampling N_x	100	100	20
Cross Range sampling N_y	100	100	20
frequency resolution, Δf	7.495MHz	7.495MHz	7.495MHz
aspect resolution $\Delta\phi$	0.0172°	0.0613°	0.0172°

Shown below are the ISAR images of the three study cases for the Bell Boeing V-22 aircraft. Figures 11, 12 and 13 represent case 1, 2 and 3 respectively.

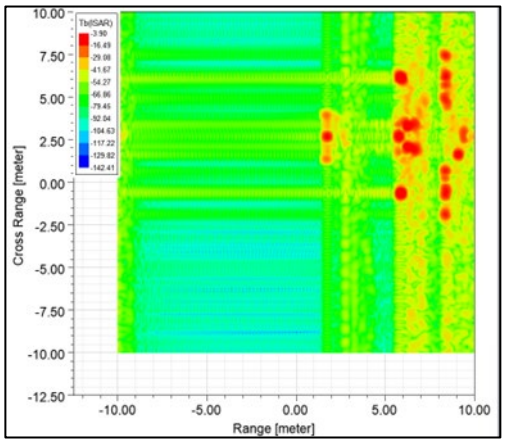

Fig. 11: First case 2-D ISAR image for a Bell Boeing V-22 aircraft.

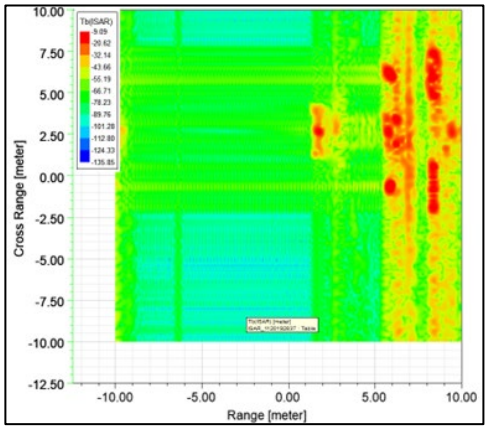

Fig. 12: 2nd case 2-D ISAR image for a Bell Boeing V-22 aircraft.

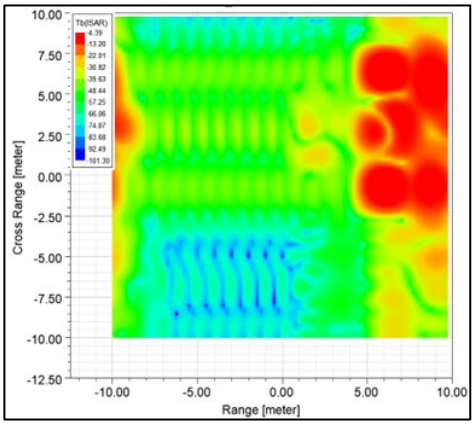

Fig. 13: 3rd case 2-D ISAR image for a Bell Boeing V-22 aircraft.

IV. Conclusion

This work has undertaken a meticulous exploration of Inverse Synthetic Aperture Radar (ISAR) imaging, shedding light on its application in the context of diverse moving targets. It covers a comprehensive overview of radar technology, emphasizing its pivotal role in modern society and particularly in military applications. The significance of radar in surveillance, target tracking, and threat detection, coupled with its indispensable role in monitoring moving targets, set the foundation for the subsequent investigation into ISAR imaging. Moreover, this study delved deep into the intricacies of ISAR, explaining its unique capability to image and analyse moving targets by utilizing their inherent motion. The discussion encompassed the methodology and implementation of ISAR imaging, providing a nuanced understanding of its principles and parameters. The focus extended to both simple and complex objects, including cubes, spheres, aircraft, fighter jets, and automotive vehicles. Through systematic simulation and analysis, the study probed three distinct cases for each object type, investigating the impact of optimum design procedures, variations in center frequency, and alterations in resolution.

The outcomes of the work underscore the critical importance of adhering to optimum design procedures for achieving high-fidelity ISAR images. The results revealed that in Case 1, where the optimum design procedure was employed, the ISAR images accurately represented the dimensions and intricate details of the objects, emphasizing the effectiveness of best practices. Conversely, intentional deviations in Cases 2 and 3, involving a decrease in center frequency and resolution, respectively, led to observable trade-offs. The examination of diverse moving targets, including cubes, spheres and aircraft, revealed common challenges and limitations associated with ISAR imaging. Notably, the study highlighted the difficulties in imaging spherical objects due to inherent limitations in obtaining a wide range of aspect angles and the symmetrical nature of these objects. The findings contribute valuable insights into the complexities of reconstructing shapes for such objects, shedding light on the impact of resolution choices, wavelength, and scattering characteristics.

References

[1] Q. Jiang, Y. Wang and J. Wang, "Design and Experimental Verification of ISAR imaging System for Airborne Maritime Surveillance Radar," 2019 6th Asia-Pacific Conference on Synthetic Aperture Radar (APSAR), Xiamen, China, 2019, pp. 1-5, doi: 10.1109/APSAR46974.2019.9048285.

[2] Moreira and Y. Huang, "A Tutorial on Synthetic Aperture Radar," in IEEE Geoscience and Remote Sensing Magazine, vol. 1, no. 1, pp. 6-43, March 2013.

[3] M.W. Van Zyl and M.R. Inggs, "Inverse Synthetic Aperture Radar Images of Moving Targets," in IEEE Transactions on Aerospace and Electronic Systems, vol. 28, no. 3, pp. 411-418, Jul. 1992.

[4] M. Farhadi, R. Feger, J. Fink, T. Wagner, and A. Stelzer, "Synthetic Aperture Radar Imaging of Moving Targets for Automotive Applications," in 2021 18th European Radar Conference (EuRAD), London, United Kingdom, 05-07 April 2022.

[5] A. Brandewie and R. Burkholder, "Passive Inverse Synthetic Aperture Radar Imaging from Non-Contiguous Frequency Bands," 2021 IEEE Radar Conference (RadarConf21), Atlanta, GA, USA, 2021, pp. 1-5, doi: 10.1109/RadarConf2147009.2021.9455223.

[6] M. A. Suliman, A. S. Emhemmed and I. A. Aref, "Suppression of Mobile Phone Radiation in Human Head Using Metamaterial," 2023 IEEE 3rd International Maghreb Meeting of the Conference on Sciences and Techniques of Automatic Control and Computer Engineering (MI-STA), Benghazi, Libya, 2023, pp. 726-731, doi: 10.1109/MI-STA57575.2023.10169491.

[7] X. Dong and Y. Zhang, "SAR/ISAR Imaing Using Commercial Millimeter-wave Radar," 2019 6th Asia-Pacific Conference on Synthetic Aperture Radar (APSAR), Xiamen, China, 2019, pp. 1-4, doi: 10.1109/APSAR46974.2019.9048497.